Heliyon 10 (2024) e25352

Contents lists available at ScienceDirect

Heliyon

journal homepage: www.cell.com/heliyon

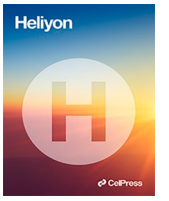

Research article

Improved stability and efficiency of inverted triple-cation mixed-halide perovskite solar cells with CsI-modified NiOx hole transporting layer

Ching-Ho Tien [a], Yu-Chen Liu [b], Thangaraji Vasudevan [b], Lung-Chien Chen [b,*]

[a] Department of Semiconductor Engineering, Lunghwa University of Science and Technology, No. 300, Sec. 1, Wanshou Rd., Taoyuan, 33306, Taiwan

[b] Department of Electro-Optical Engineering, National Taipei University of Technology, No. 1, Sec. 3, Chung-Hsiao E. Rd., Taipei, 10608, Taiwan

ARTICLE INFO

Keywords:
Perovskites
CsI
Passivation
Interface engineering
Perovskite solar cell

ABSTRACT

Addressing the critical challenge of mitigating defect generation and enhancing the extended durability of perovskite solar cells (PeSCs) requires effective passivation materials. In our study, we investigated the impact of varying concentrations of cesium iodide (CsI), an alkali halide, on the interface layer among the hole transporting layer (HTL) and the perovskite film in a triple-cation lead hybrid halide $Cs_{0.15}FA_{0.81}MA_{0.04}Pb(I_{2.86}Br_{0.14})_3$ perovskite layer. Our findings revealed that the introduction of CsI into the NiOx HTL led to improved crystallinity and a reduction in defects within the perovskite film. Consequently, the photovoltaic performance of the CsI-modified PeSC exhibited a notable enhancement. Specifically, the photoelectric conversion efficiency (PCE) increased from 18.7 % in the original PeSC, which lacked CsI modification, to 20.5 %. Moreover, this improvement in PCE was accompanied by excellent stability, with the CsI-modified PeSC retaining 80 % of its opening PCE even afterward 144 h of testing.

1. Introduction

Throughout the span of ten years, organic-inorganic halide perovskites have risen to prominence as exceptional photovoltaic materials, primarily owing to their remarkable attributes such as superior light absorption capabilities, high carrier mobility, minimal trap state density, and extended electron-hole diffusion distances. This development has led to a notable improvement in the photoelectric conversion efficiency (PCE) of perovskite solar cells (PeSCs) devices, increasing from 3.8 to 25.8 % [1–3], positioning them on par with commercially available silicon-based solar cell devices.

In the realm of inverted planar PeSCs, the hole transporting layer (HTL), serving as the initial functional layer, plays a multifaceted role. It primarily serves to impede the movement of electrons (−) while facilitating the transport of holes (+), ushering them toward the electrodes, thereby ensuring effective electron-hole separation. Concurrently, the usage of HTL materials allows for the fine-tuning of interface energy levels and the enhancement of Schottky barrier contacts among the perovskite layer and the anode, both of which significantly influence PeSC performance. In contemporary research, there are various techniques available for producing NiOx hole transporting layers (HTL) [4]. These methods generally fall into two categories: physical vapor deposition and chemical solution

* Corresponding author.
E-mail addresses: chtien@mail.lhu.edu.tw (C.-H. Tien), gunsmoke0487@gmail.com (Y.-C. Liu), orgthangaraji@gmail.com (T. Vasudevan), ocean@ntut.edu.tw (L.-C. Chen).

https://doi.org/10.1016/j.heliyon.2024.e25352
Received 25 July 2023; Received in revised form 10 January 2024; Accepted 25 January 2024
Available online 28 January 2024

processing [5]. Historically, HTL films (NiOx) have been generated via multiple methods, including pulsed laser deposition (PLD) [6], magnetron sputtering deposition [7], atomic-layer deposition (ALD) [8], and electron beam (e-beam) evaporation [9], among others. Nonetheless, the physical vapor deposition method usually demands costly high-vacuum equipment, leading to an escalation in the overall cost of depositing films. In contrast, solution processing methods present a more cost-effective and convenient route for producing NiOx thin films [10]. Thus far, HTL materials for inverted planar PeSCs can be characterized into two main groups: organic and inorganic. Among the organic hole transporting materials (HTMs), common examples include PTAA [11,12] and PEDOT:PSS [13,14]. However, these materials present challenges due to their intricate synthesis processes, demanding conditions, purification difficulties, and associated costs. Furthermore, they exhibit limited hole mobility and often require the addition of dopants, with the hygroscopic and corrosive nature of these dopants posing stability concerns for the devices. Consequently, there is a pressing need to identify stable and alternative HTMs. In the realm of inorganic HTMs, examples include CuSCN [15,16], CuI [17,18], Cu2O [19,20], and NiOx [21,22]. Inorganic HTL materials have garnered significant attention because of their advantages, including high chemical durability, versatile and straightforward process methods, excellent optical transparency, and cost-effectiveness. Among these, NiOx-based PeSCs have shown promise in achieving high photoelectric conversion efficiencies (PCEs) and have gained widespread use. For instance, in 2014, Jeng et al. pioneered the application of NiOx as an HTL in PeSCs, achieving a PCE of 7.8 % [13]. In 2019, Liyuan Han et al. introduced 3,5-difluoro-2,5,7,7,8,8-hexacyanoquinodimethane (F2HCNQ) modification to NiOx, achieving a remarkable PCE of 22.13 % on an inverted rigid substrate [23].

Surface modification serves as a straightforward approach to fine-tuning the surface characteristics of thin films, effectively enhancing their wettability and chemical interactions. This, in turn, leads to improvements in the crystalline properties of perovskite films, the passivation of the surface and interface defects, and the regulation of interface energy level alignments. Various agents, including organic molecules [24–26], alkali chlorides [27], optical plastics [28], and ozone [29,30], have been employed for the surface modification of NiOx. Chen et al. introduced the organic molecule ferrocene dicarboxylic acid (FDA) for NiOx modification, leading to notable enhancements in perovskite film crystallinity and a reduction in carrier recombination [25]. Consequently, the NiOx-based inverted PeSC modified with the FDA achieved a final photoelectric conversion efficiency (PCE) of 18.20 %. He et al. chose alkali chloride to modify NiOx and observed that the addition of a KCl layer (buffer) facilitated the formation of an ordered interface between NiOx and the perovskite layer [27]. This efficiently reduced surface defects on the perovskite film, resulting in the open-circuit voltage (Voc) increased from 1.07 to 1.15 eV, with a PCE approaching 21 %. Shen et al. utilized an optical plastic, bilateral polystyrene passivation layer to successfully passivate perovskite/HTL and perovskite/ETL interface trap states [28]. This approach resulted in a high open-circuit voltage (Voc) of 1.149 V and a notable PCE of 19.9 %. Additionally, Shen et al. employed ultraviolet/ozone (UVO) treatment on NiOx for varying durations to adjust the stoichiometric ratio of Ni/O in NiOx and enhance film conductivity and wettability [30]. This treatment also led to energy band shifts, aligning the valence band maximum (VBM) more closely with the perovskite active layer. Following UVO treatment, the work function of the prepared NiOx thin film increased from 4.79 to 4.86 eV, and the VBM shifted from −5.27 to −5.34 eV.

In this study, we introduced a modification layer consisting of CsI, an alkali metal halide, strategically positioned among the NiOx and the perovskite active layer to enhance their interfacial interactions. The investigation revealed that the incorporation of the CsI-modified layer effectively alleviated interfacial stress through a well-balanced combination of optimized materials selection, thermal annealing, and interface engineering. This comprehensive approach yielded an improved property of the perovskite device, characterized by higher grain sizes. Consequently, this modification led to improved charge extraction and inhibited charge recombination. The net result was the successful creation of a perovskite solar cell (PeSC) characterized by exceptional device reliability, culminating in an impressive photoelectric conversion efficiency (PCE) of 20.5 %.

2. Experimental

2.1. Essential materials

CsBr (Cesium bromide, 99.9 %), CsI (Cesium iodide, 99.99 %), PbI2 (lead iodide, 99.99 %), nickel(II) nitrate (99.99 %), $C_2H_8N_2$ (ethylenediamine, 99 %), and $C_2H_6O_2$ (ethylene glycol, 99 %) were procured from Alfa Aesar. FAI (Formamidinium iodide, 99.55 %), MABr (methylammonium bromide, 99.55 %), and BCP (bathocuproin, 99.5 %) were obtained from Lumtec. DMSO (Dimethyl sulfoxide, 99.55 %), DMF (N, N-dimethyl formamide, 99.55 %), and C60 (fullerene, 99.9 %) were sourced from Uni-Onward. Acquired from Ruilong, the FTO glass substrate with a patterned structure has a sheet resistance of 7 Ω/sq.

2.2. Film formation and device fabrication

FTO glass substrates underwent a sequential ultrasonic cleaning process with acetone, ethanol, and isopropanol for 15 min each, after that drying and treatment in a UV ozone oven for 15 min. The precursor for the NiOx hole transport layer (HTL) was prepared by dissolving 2.91 g of nickel nitrate in 10 mL of ethylene glycol ($C_2H_6O_2$), to which 0.67 mL of ethylenediamine ($C_2H_8N_2$) was added. This mixture was stirred overnight at 25 °C. The NiOx HTL was then spin-coated onto the glass substrate (FTO) at 3000 rpm for 45 s and subjected to a secondary annealing process at 120 °C for 10 min and 300 °C for 60 min. For the formulation of CsI modification layer solutions, CsI powder was dissolved in a combination of IPA and deionized water solvents, yielding various concentrations of 0, 5, 10, 15, and 20 $mgmL^{-1}$. A thin layer of CsI modification was then spin-coated onto the NiOx-covered FTO substrates at 3000 rpm for 30 s within a nitrogen-filled glovebox.

The photoactive precursor solution for the $Cs_{0.15}FA_{0.81}MA_{0.04}Pb(I_{2.86}Br_{0.14})_3$ perovskite was prepared by dissolving MABr (4.47

mg), CsBr (21.2 mg), CsI (13 mg), FAI (139 mg), and PbI_2 (461 mg) in a mixed solvent of DMSO/DMF (1:4, v/v) at room temperature for at least 22 h. Subsequently, 80 μl of the photoactive perovskite solution was deposited via spin coating at 1000 rpm and 5000 rpm for 10 and 30 s, respectively. During the last 20 s of the second step, 100 μl of toluene was drop-casted onto the substrate. The resulting perovskite films on pure NiOx or CsI-modified NiOx layers were then dried on a hot plate at 100 °C for 10 min to form the $Cs_{0.15}FA_{0.81}MA_{0.04}Pb(I_{2.86}Br_{0.14})_3$ perovskite photoactive film. Following this, the electron transporting layer and electron blocking layer were consecutively coated by thermal evaporation of C_{60} and BCP under high vacuum conditions. The PeSC devices were finalized by thermally evaporating a thick layer of Ag (100 nm) to form the top electrode. All PeSC devices had an active area of 4 mm^2 as distinct by the metal mask.

The architecture of the PeSC device with the CsI modification layer is illustrated in Fig. 1a, with the CsI-altered NiOx layer measuring approximately 30 nm and the $Cs_{0.15}FA_{0.81}MA_{0.04}Pb(I_{2.86}Br_{0.14})_3$ perovskite photoactive layer thickness estimated at ≈ 450 nm (Fig. 1b). The incorporation of the CsI modification layer optimizes the interface between the NiOx (HTL) and the perovskite photoactive layer, enhances the quality of the large-grained perovskite film, diminished interface defects and traps, and improves charge extraction and transport.

2.3. Materials and device characterization

The morphology of the perovskite solar cell (PeSC) film and the cross-sectional structure of the PeSC device were examined using a field-emission scanning electron microscope (FESEM, Sigma, ZEISS, Germany). X-ray diffraction (XRD) study was conducted with an

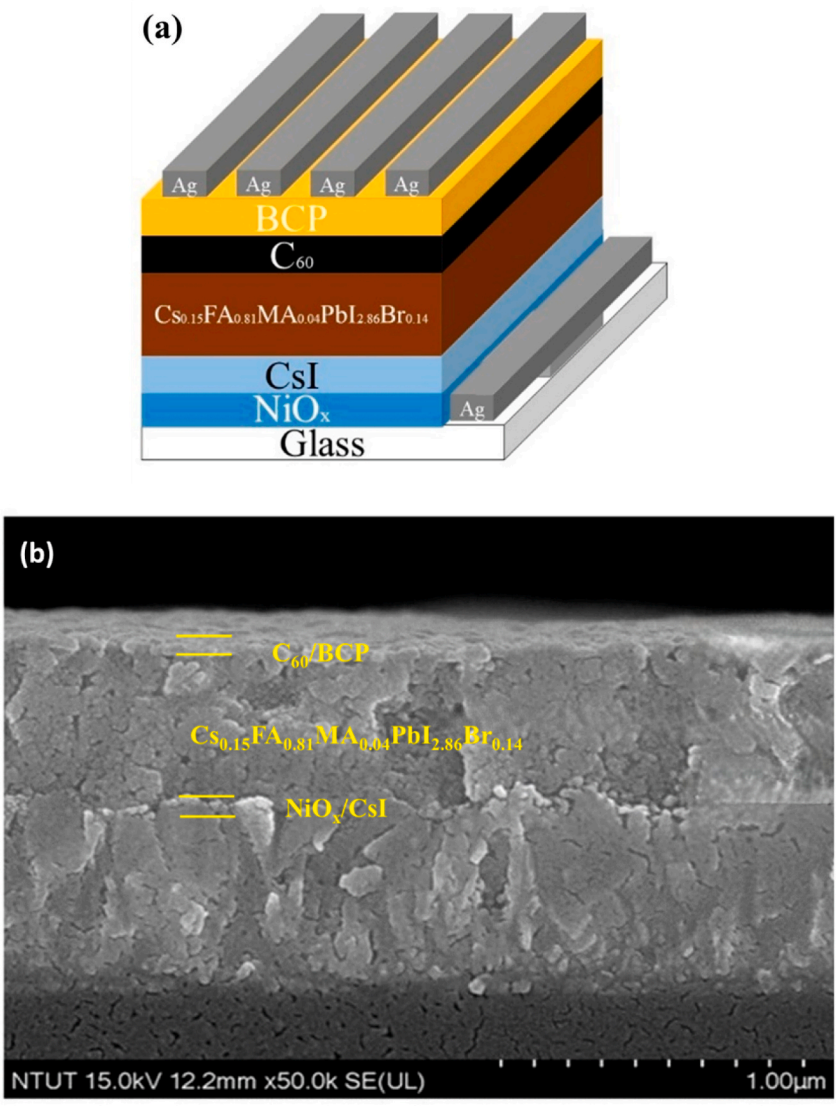

Fig. 1. (a) The inverted PeSC device architecture, (b) SEM cross-sectional image.

X-ray diffractometer (X'Pert PRO MRD, PANalytical, Netherlands). UV-VIS absorption and photoluminescence (PL) spectra were recorded by a UV–vis–near infrared spectrophotometer (Jasco, Japan, V-770) and a fluorescence spectrometer (Hitachi, Japan, F-7000), respectively. Photovoltaic performance measurements were conducted employing a solar cell simulator (Basic-MFS-PV, Hong-Ming Technology Co., Ltd., Taiwan) operating under AM 1.5 G standard sunlight, and a Keithley-2400 source meter was used for characterization. The luminous intensity of the solar cell simulator, set at 100 mW/cm^2, was standardized by a typical silicon solar cell (PV Measurements Inc., USA, PVM-894).

3. Results and discussion

In this study, various CsI concentrations, namely 0, 5, 10, 15, and 20 mg/mL, were utilized to modify the films, denoted as CsI-0, CsI-5, CsI-10, CsI-15, and CsI-20, respectively. Fig. 2a displays the current density-voltage (J-V) curves for PeSC devices treated with various concentrations of CsI-modified layers, while Table 1 provides an overview of the extracted photovoltaic parameters for these devices. Notably, the PeSC device treated with 10 mg/mL CsI achieved the most impressive performance, featuring a short-circuit current density (Jsc) of 25.0 mA/cm^2, an open-circuit voltage (Voc) of 1.06 V, a fill factor (FF) of 78.5 %, a power conversion efficiency (PCE) of 20.5 %, and a stabilized maximum power point (MPP) of 20.4 %. This represents a significant enhancement compared to the unmodified device (CsI-0), which exhibited a PCE of 18.7 %, Jsc of 24.5 mA/cm^2, Voc of 1.04 V, and FF of 73.0 %.

The observed increase in Jsc and FF in CsI-modified devices can be attributed to the effective enhancement of perovskite film crystallinity through CsI-modified NiOx, leading to a reduction in interfacial defects and associated carrier recombination, which will be explain in detail later. Fig. 2b further examined the device integrated Jsc through EQE (external quantum efficiency) measurements, with the 10 mg/mL CsI treatment concentration selected due to its good performance. These measurements revealed a significant boost in quantum efficiency for CsI-modified NiOx PeSCs in the wavelength reach from 500 to 800 nm, signifying efficient photon-to-electrical energy conversion. The integrated current based on the EQE curve reveals that the device modified with CsI-10 attains a higher Jsc of 24.5 mA/cm2 compared to the unmodified device.

In Fig. 3, the XRD pattern of CsI-modified perovskite films is depicted. Both films, with and without the CsI modification layer, exhibit three prominent diffraction peaks at (110), (220), and (310), with a slight increase in the intensity of these peaks in the CsI-

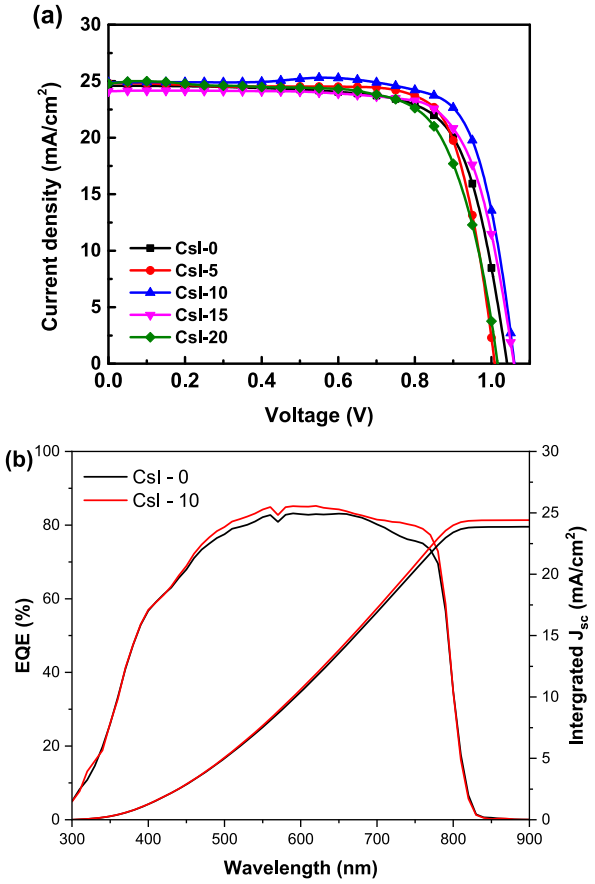

Fig. 2. (a) Current density vs. voltage curves (J–V) and (b) external quantum efficiency (EQE) spectra and Integrated Jsc values of PeSCs based on different concentrations of CsI-modified NiO_x HTL.

Table 1
Summarized the performance metrics of PeSCs with varied CsI solution concentrations.

Sample	Jsc (mA cm^{-2})	Voc (V)	FF (%)	PCE (%)
CsI-0	24.5	1.04	73.0	18.7
CsI-5	24.8	1.01	76.9	19.3
CsI-10	25.0	1.06	78.5	20.5
CsI-15	24.3	1.06	75.2	19.4
CsI-20	24.8	1.02	72.0	18.2
CsI-10 (MPP)	–	–	–	20.4

modified perovskite pattern. Moreover, when compared to the perovskite film lacking CsI modification (FWHM = 0.315), the perovskite film modified with NiOx HTL at a 10 mg/mL CsI concentration demonstrates superior crystal characteristics, evidenced by a narrower full width at half maximum (FWHM = 0.225). This suggests a reduction in crystal defects and structural flaws in the perovskite film. However, as the CsI concentration is elevated to 15 and 20 $mgmL^{-1}$, the intensity of the perovskite film crystal phase (110) starts to decrease. This phenomenon may arise from an excess of Cs cations, which could lead to reduced crystallinity, resulting in increased surface pores and film defects.

Fig. 4 showcases scanning electron microscopy (SEM) images of perovskite films, both with and without CsI modification. To compare Fig. 4a and b, the CsI modification makes some of pores on the surface of perovskite film. The observations reveal that the perovskite film's surface, when treated with CsI at a concentration of 10 $mgmL^{-1}$, as shown in Fig. 4c, exhibited fewer pores and larger average grain sizes. This suggests that CsI modification on the NiOx surface is conducive to enhancing the crystallinity and coverage of the perovskite film. However, at CsI concentrations of 15 and 20 mg/mL, as shown in Fig. 4d and e, an excessive presence of Cs ions led to an increase in pore formation and a noticeable variation in average grain size, indicating poorer film quality at these concentrations.

Fig. 5a depicts the absorption spectra of perovskite films with varying concentrations of CsI-modified NiOx as the hole transport layer (HTL). The results highlight that the perovskite film treated with a 10 mg/mL CsI concentration exhibits the highest intensity in its absorption spectrum. This indicates superior crystallinity, compactness, extensive coverage, uniform grain distribution, and optimal assembly efficiency for PeSCs. CsI modification of NiOx primarily enhances the contact area between the HTL and the perovskite light-absorbing layer, facilitating carrier extraction, reducing recombination effects, and achieving a balanced carrier transport, thereby improving optoelectrical performance. However, at concentrations of 15 and 20 mg/mL, the film's absorption and overall device efficiency decrease due to an excessive presence of Cs ions on the film's surface. Fig. 5b reveals a significant increase in photoluminescence (PL) intensity for the perovskite film after passivation treatment with 10 mg/mL CsI-modified NiOx. This result demonstrates effective passivation of film quality and crystallinity, along with the suppression of non-radiative recombination within the film.

To examine the impact of the CsI modification layer on device stability, we monitored PCE degradation for both the CsI-modified and control devices under 25 °C and AM1.5G standard sunlight conditions. The control device exhibited a significant decline of more than 30 % in PCE after 144 h of operation, whereas the CsI-modified device maintained an impressive 80 % of its initial efficiency (see Fig. 6). This observation highlights that the CsI-modified perovskite film not only enhances the interface contact between the HTL and perovskite active layer, improving perovskite film quality and increasing device PCE [31,32], but also offers effective moisture and oxygen resistance, thereby enhancing the stability of PeSCs [33].

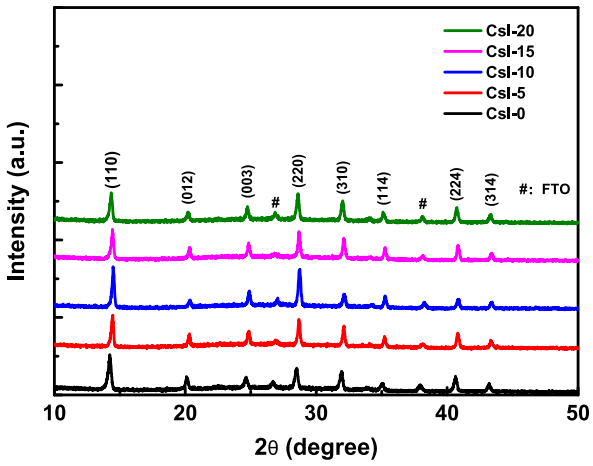

Fig. 3. XRD patterns of the perovskite thin films based on different concentrations of CsI-modified NiO_x (HTL).

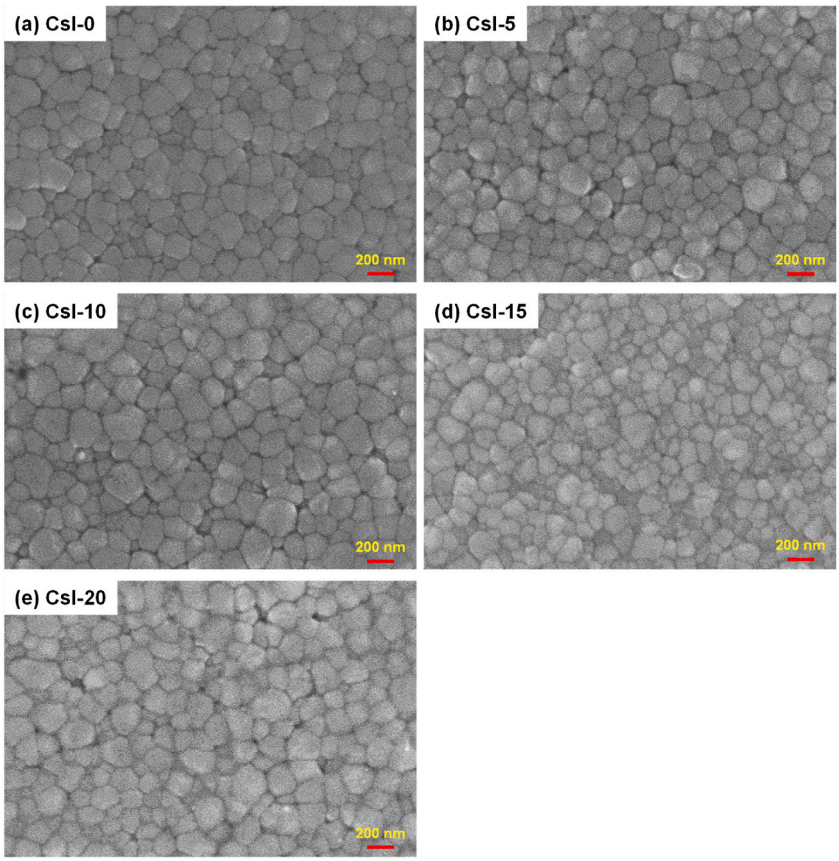

Fig. 4. SEM images of the perovskite films based on different concentrations of CsI-modified NiO_x HTL.

4. Conclusion

To summarize, this study introduces a novel approach to enhance the heterostructure contact (NiOx/perovskite) among the hole transport layer (HTL) and the perovskite absorber layer, incorporating a CsI buffer layer. This modification technique leads to notable improvements in the perovskite film's light absorption and crystallinity. Specifically, when applying a 10 mg/mL CsI layer on NiOx, the power conversion efficiency (PCE) of the PeSC device improved to 20.5 %, while maintaining 80 % of its opening PCE even after 144 h of storage. These results highlight the significant role of CsI in enhancing charge extraction and transfer, as well as reducing interfacial trap and defect-related recombination processes. Consequently, this contributes to heightened device stability and improved photovoltaic properties.

Notes

The authors have no conflicts of interest related to financial matters.

Data availability statement

All the data are fully available without restrictions.

Additional information

No additional information is available for this paper.

CRediT authorship contribution statement

Ching-Ho Tien: Writing – original draft, Investigation, Funding acquisition, Formal analysis, Conceptualization. **Yu-Chen Liu:** Methodology, Investigation, Data curation. **Thangaraji Vasudevan:** Writing – original draft, Investigation, Formal analysis. **Lung-Chien Chen:** Writing – review & editing, Supervision, Funding acquisition, Formal analysis, Conceptualization.

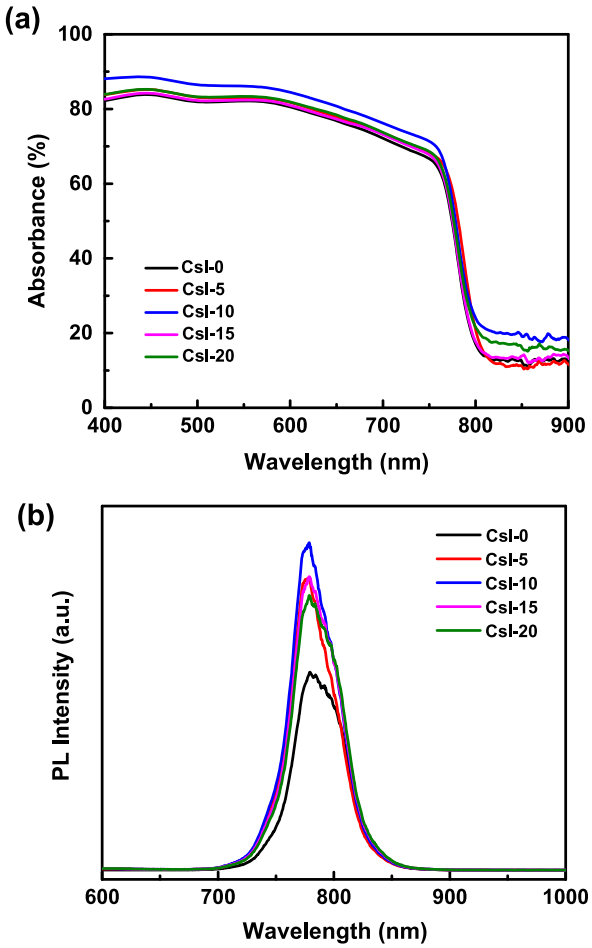

Fig. 5. (a) Absorption and (b) PL spectra of the perovskite films based on different concentrations of CsI-modified NiO_x (HTL).

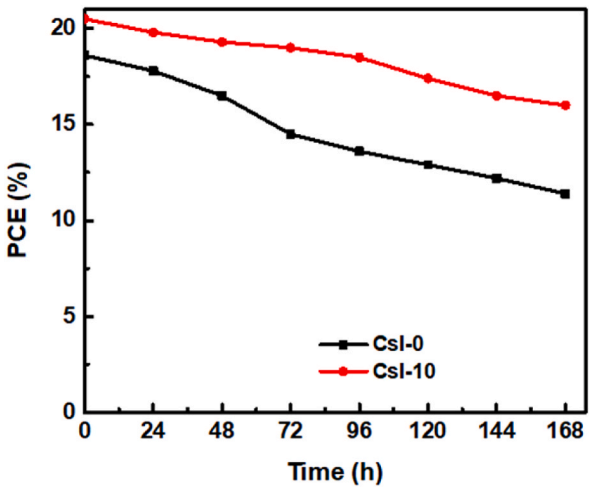

Fig. 6. PCE stability in N_2 glovebox for PeSCs with and without CsI.

Declaration of competing interest

The authors declare that they have no known competing financial interests or personal relationships that could have appeared to influence the work reported in this paper.

Acknowledgements

The National Science and Technology Council (Taiwan) provided support for this research under Contract Nos. 111-2221-E-027-040-MY3 and 111-2221-E-262-006.

References

[1] A. Kojima, K. Teshima, Y. Shirai, T. Miyasaka, Organometal halide perovskites as visible-light sensitizers for photovoltaic cells, J. Am. Chem. Soc. 131 (17) (2009) 6050–6051, https://doi.org/10.1021/ja809598r.
[2] H. Min, D.Y. Lee, J. Kim, G. Kim, K.S. Lee, J. Kim, M.J. Paik, Y.K. Kim, K.S. Kim, M.G. Kim, T.J. Shin, S.I. Seok, Perovskite solar cells with atomically coherent interlayers on SnO_2 electrodes, Nature 598 (7881) (2021) 444–450, https://doi.org/10.1038/s41586-021-03964-8.
[3] Best Research-Cell Efficiencies, National Renewable Energy Laboratory, https://www.nrel.gov/pv/assets/pdfs/best-research-cell-efficiencies.pdf (Rev. 04-05-2023).
[4] D. Di Girolamo, F. Di Giacomo, F. Matteocci, A.G. Marrani, D. Dini, A. Abate, Progress, highlights and perspectives on NiO in perovskite photovoltaics, Chem. Sci. 11 (2020) 7746–7759, https://doi.org/10.1039/D0SC02859B.
[5] F. Ma, Y. Zhao, J. Li, X. Zhang, H. Gu, J. You, "Nickel oxide for inverted structure perovskite solar cells,'', J. Energy Chem. 52 (2021) 393–411, https://doi.org/10.1016/j.jechem.2020.04.027.
[6] Z. Qiu, H. Gong, G. Zheng, S. Yuan, H. Zhang, X. Zhu, H. Zhou, B. Cao, "Enhanced physical properties of pulsed laser deposited NiO films via annealing and lithium doping for improving perovskite solar cell efficiency,'', J. Mater. Chem. C 5 (2017) 7084–7094, https://doi.org/10.1039/C7TC01224A.
[7] G. Li, Y. Jiang, S. Deng, A. Tam, P. Xu, M. Wong, H.S. Kwok, "Overcoming the Limitations of sputtered nickel oxide for high-efficiency and large-area perovskite solar cells,'', Adv. Sci. 4 (2017) 1700463 (Weinh).
[8] B. Zhao, L.C. Lee, L. Yang, A.J. Pearson, H. Lu, X.J. She, L. Cui, K.H.L. Zhang, R.L.Z. Hoye, A. Karani, P. Xu, A. Sadhanala, N.C. Greenham, R.H. Friend, J. L. MacManus-Driscoll, "In situ Atmospheric deposition of Ultrasmooth nickel oxide for efficient perovskite solar cells,'' D. Di, ACS Appl. Mater. Interfaces 10 (2018) 41849–41854, https://doi.org/10.1021/acsami.8b15503.
[9] S. Pang, C. Zhang, H. Dong, D. Chen, W. Zhu, H. Xi, J. Chang, Z. Lin, J. Zhang, Y. Hao, Efficient NiOx hole transporting layer obtained by the Oxidation of metal nickel film for perovskite solar cells, ACS Appl. Energy Mater. 2 (2019) 4700–4707, https://doi.org/10.1021/acsaem.9b00169.
[10] L. Li, W. Shen, C. Yang, Y. Dou, X. Zhu, Y. Dong, J. Zhao, J. Xiao, F. Huang, Y.B. Cheng, J. Zhong, In-situ monitored chemical bath deposition of planar NiOx layer for inverted perovskite solar cell with enhanced efficiency, J. Mater. Sci. Technol. 133 (2023) 145–153, https://doi.org/10.1016/j.jmst.2022.05.038.
[11] Y. Kim, E.H. Jung, G. Kim, D. Kim, B.J. Kim, J. Seo, Sequentially fluorinated PTAA polymers for enhancing V_{OC} of high-performance perovskite solar cells, Adv. Energy Mater. 8 (29) (2018) 1801668, https://doi.org/10.1002/aenm.201801668.
[12] M. Wang, H. Wang, W. Li, X. Hu, K. Sun, Z. Zang, Defect passivation using ultrathin PTAA layers for efficient and stable perovskite solar cells with a high fill factor and eliminated hysteresis, J. Mater. Chem. A 7 (16) (2019) 26421–26428, https://doi.org/10.1039/C9TA08314F.
[13] J.Y. Jeng, K.C. Chen, T.Y. Chiang, P.Y. Lin, T.D. Tsai, Y.C. Chang, T.F. Guo, P. Chen, T.C. Wen, Y.J. Hsu, Nickel oxide electrode interlayer in $CH_3NH_3PbI_3$ perovskite/PCBM planar-heterojunction hybrid solar cells, Adv. Mater. 26 (4) (2014) 4107–4113, https://doi.org/10.1002/adma.201306217.
[14] J. Seo, S. Park, Y.C. Kim, N.J. Jeon, J.H. Noh, S.C. Yoon, S.I. Seok, Benefits of very thin PCBM and LiF layers for solution-processed p–i–n perovskite solar cells, Energy Environ. Sci. 7 (8) (2014) 2642–2646, https://doi.org/10.1039/C4EE01216J.
[15] M. Lyu, J. Chen, N.G. Park, Improvement of efficiency and stability of CuSCN-based inverted perovskite solar cells by post-treatment with potassium thiocyanate, J. Solid State Chem. 269 (2019) 367–374, https://doi.org/10.1016/j.jssc.2018.10.014.
[16] T.-H. Chowdhury, M. Akhtaruzzaman, M.E. Kayesh, R. Kaneko, T. Noda, J.J. Lee, A. Islam, Low temperature processed inverted planar perovskite solar cells by r-GO/CuSCN hole-transport bilayer with improved stability, Sol. Energy 171 (2018) 652–657, https://doi.org/10.1016/j.solener.2018.07.022.
[17] W. Sun, S. Ye, H. Rao, Y. Li, Z. Liu, L. Xiao, Z. Chen, Z. Bian, C. Huang, Room-temperature and solution-processed copper iodide as the hole transport layer for inverted planar perovskite solar cells, Nanoscale 8 (35) (2016) 15954–15960, https://doi.org/10.1039/C6NR04288K.
[18] D.-B. Khadka, Y. Shirai, M. Yanagida, K. Miyano, Ammoniated aqueous precursor ink processed copper iodide as hole transport layer for inverted planar perovskite solar cells, Sol. Energy Mater. Sol. Cell. 210 (2020) 110486, https://doi.org/10.1016/j.solmat.2020.110486.
[19] L. Lin, L. Jiang, P. Li, B. Fan, Y. Qiu, A modeled perovskite solar cell structure with a Cu_2O hole-transporting layer enabling over 20% efficiency by low-cost low-temperature processing, J. Phys. Chem. Solids 124 (2019) 205–211, https://doi.org/10.1016/j.jpcs.2018.09.024.
[20] S. Sajid, S. Alzahmi, I.-B. Salem, I.M. Obaidat, Guidelines for fabricating highly efficient perovskite solar cells with Cu_2O as the hole transport material, Nanomaterials 12 (19) (2022) 3315, https://doi.org/10.3390/nano12193315.
[21] M. Yanagida, T. Nakamura, T. Yoshida, D.-B. Khadka, Y. Shirai, K. Miyano, Surface modification of sputtered NiOx hole transport layer for $CH_3NH_3PbI_3$ perovskite solar cells, Jpn. J. Appl. Phys. 62 (2023) SK1054, https://doi.org/10.35848/1347-4065/acd5dc.
[22] T. Wu, L.K. Ono, R. Yoshioka, C. Ding, C. Zhang, S. Mariotti, J. Zhang, K. Mitrofanov, X. Liu, H. Segawa, R. Kabe, L. Han, Y. Qi, Elimination of light-induced degradation at the nickel oxide-perovskite heterojunction by aprotic sulfonium layers towards long-term operationally stable inverted perovskite solar cells, Energy Environ. Sci. 15 (11) (2022) 4612–4624, https://doi.org/10.1039/D2EE01801B.
[23] P. Ru, E. Bi, Y. Zhang, Y. Wang, W. Kong, Y. Sha, W. Tang, P. Zhang, Y. Wu, W. Chen, X. Yang, H. Chen, L. Han, High electron affinity enables fast hole extraction for efficient flexible inverted perovskite solar cells, Adv. Energy Mater. 10 (12) (2020) 1903487, https://doi.org/10.1002/aenm.201903487.
[24] J. He, Y. Xiang, F. Zhang, J. Lian, R. Hu, P. Zeng, J. Song, J. Qu, Improvement of red light harvesting ability and open circuit voltage of Cu:NiO_x based p-i-n planar perovskite solar cells boosted by cysteine enhanced interface contact, Nano Energy 45 (2018) 471–479, https://doi.org/10.1016/j.nanoen.2018.01.017.
[25] J. Zhang, H. Luo, W. Xie, X. Lin, X. Hou, J. Zhou, S. Huang, W. Ou-Yang, Z. Sun, X. Chen, Efficient and ultraviolet durable planar perovskite solar cells via a ferrocenecarboxylic acid modified nickel oxide hole transport layer, Nanoscale 10 (12) (2018) 5617–5625, https://doi.org/10.1039/C7NR08750K.
[26] S. Wang, Y. Zhu, C. Wang, R. Ma, NH_4F as an interfacial modifier for high performance NiOx-based inverted perovskite solar cells, Org. Electron. 78 (2020) 105627, https://doi.org/10.1016/j.orgel.2020.105627.
[27] W. Chen, Y. Zhou, G. Chen, Y. Wu, B. Tu, F.Z. Liu, L. Huang, A.M.C. Ng, A.B. Djurišić, Z. He, Alkali chlorides for the suppression of the interfacial recombination in inverted planar perovskite solar cells, Adv. Energy Mater. 9 (19) (2019) 1803872, https://doi.org/10.1002/aenm.201803872.
[28] T. Wang, Z. Cheng, Y. Zhou, H. Liu, W. Shen, Highly efficient and stable perovskite solar cells via bilateral passivation layers, J. Mater. Chem. A 7 (38) (2019) 21730–21739, https://doi.org/10.1039/C9TA08084H.
[29] Y. Sun, W. Chen, Y. Wu, Z. He, S. Zhang, S. Chen, A low-temperature-annealed and UV-ozone-enhanced combustion derived nickel oxide hole injection layer for flexible quantum dot light-emitting diodes, Nanoscale 11 (3) (2019) 1021–1028, https://doi.org/10.1039/C8NR08976K.
[30] T. Wang, D. Ding, H. Zheng, X. Wang, J. Wang, H. Liu, W. Shen, Efficient inverted planar perovskite solar cells using ultraviolet/ozone-treated NiOx as the hole transport layer, Sol. RRL 3 (6) (2019) 1900045, https://doi.org/10.1002/solr.201900045.

[31] W. Li, J. Li, G. Niua, L. Wang, Effect of cesium chloride modification on the film morphology and UV-induced stability of planar perovskite solar cells, J. Mater. Chem. A 4 (30) (2016) 11688–11695, https://doi.org/10.1039/C5TA09165A.
[32] Y. Bai, H. Chen, S. Xiao, Q. Xue, T. Zhang, Z. Zhu, Q. Li, C. Hu, Y. Yang, Z. Hu, F. Huang, K.S. Wong, H.-L. Yip, S. Yang, Effects of a molecular monolayer modification of NiO nanocrystal layer surfaces on perovskite crystallization and interface contact toward faster hole extraction and higher photovoltaic performance, Adv. Funct. Mater. 26 (17) (2016) 2950–2958, https://doi.org/10.1002/adfm.201505215.
[33] J. You, L. Meng, T.-B. Song, T.-F. Guo, Y. Michael Yang, W.-H. Chang, Z. Hong, H. Chen, H. Zhou, Q. Chen, Y. Liu, N. De Marco, Y. Yang, Improved air stability of perovskite solar cells via solution-processed metal oxide transport layers, Nat. Nanotechnol. 11 (2016) 75–81, https://doi.org/10.1038/nnano.2015.230.